Acta Mech. Sin. (2011) 27(3):330–338
DOI 10.1007/s10409-011-0460-x

RESEARCH PAPER

Shear flow induced vibrations of long slender cylinders with a wake oscillator model

Fei Ge · Wei Lu · Lei Wang · You-Shi Hong

Received: 3 February 2010 / Revised: 7 April 2010 / Accepted: 26 August 2010

Abstract A time domain model is presented to study the vibrations of long slender cylinders placed in shear flow. Long slender cylinders such as risers and tension legs are widely used in the field of ocean engineering. They are subjected to vortex-induced vibrations (VIV) when placed within a transverse incident flow. A three dimensional model coupled with wake oscillators is formulated to describe the response of the slender cylinder in cross-flow and in-line directions. The wake oscillators are distributed along the cylinder and the vortex-shedding frequency is derived from the local current velocity. A non-linear fluid force model is accounted for the coupled effect between cross-flow and in-line vibrations. The comparisons with the published experimental data show that the dynamic features of VIV of long slender cylinder placed in shear flow can be obtained by the proposed model, such as the spanwise average displacement, vibration frequency, dominant mode and the combination of standing and traveling waves. The simulation in a uniform flow is also conducted and the result is compared with the case of non-uniform flow. It is concluded that the flow shear characteristic has significantly changed the cylinder vibration behavior.

Keywords Vortex-induced vibration · Vortex-induced wave · Shear flow · Wake oscillator · Long slender cylinder

The project was supported by the National Natural Science Foundation of China (10532070), the Knowledge Innovation Program of Chinese Academy of Sciences (KJCX2-YW-L07) and the LNM Initial Funding for Young Investigators.

F. Ge · W. Lu · L. Wang · Y.-S. Hong (✉)
State Key Laboratory of Nonlinear Mechanics,
Institute of Mechanics, CAS,
100190 Beijing, China
e-mail: hongys@imech.ac.cn

1 Introduction

Long slender cylinders, such as marine risers, tension-leg platform tendons and mooring or towing cables are subjected to vortex-induced vibrations (VIV) when placed within a transverse oncoming flow. The most undesirable form of VIV for the offshore structures is termed lock-in, which describes the ability of an elastic structure to control the shedding process in a bandwidth around its resonant frequency. Associated with lock-in is large amplitude excitation which has the potential to cause damaging fatigue failure. Lock-in may occur at certain velocities of uniform flow conditions. However, for spatially sheared flow conditions, the occurrence of lock-in is more complicated [1]. In the ocean, cylinders are generally exposed to a shear current profile over their depth and hence the prediction of those VIV is an important subject of research especially for cylinders with very large aspect ratio (Length/Diameter$\sim 10^3$), which have been widely used in oil fields of deep waters.

A number of methods for predicting the dynamic behavior of structures subjected to VIV are available in literature, most of which are discussed in the comprehensive reviews due to Sarpkaya [2], Williamson and Govardhan [3], Gabbai and Benaroya [4] and Chaplin et al. [5]. Models based on Navier-Stocks equations use the method of computational fluid dynamics (CFD) to determine the fluid motions and pressures, and hence to determine the hydrodynamic forces acting on the cylinder. Such models need to be coupled to a structure model which computes structural displacements and hence the new fluid boundary conditions. This approach is extremely computationally demanding and has not so far been applied for practical problems. Another method is to model the principle features of vortex shedding in the cylinder wake using a dynamical system. The main difference between this phenomenological approach and CFD is that the dynamic behavior of fluid in the cylinder

wake is modeled instead of being computed. Facchinetti et al. [6] verified the effect of cylinder movement on the lift fluctuation via different types of coupling terms (displacement, velocity and acceleration). They came up with a formulation of the wake oscillator model that was qualitatively and, to some extent, quantitatively able to reproduce aspects of VIV observed experimentally for rigid cylinders elastically supported and for flexible cylinders. Some parameters in wake oscillator model, however, have to be derived from tests.

Most attention of related researches has been put on cylinder VIV in cross-flow (CF). The main reasons for not considering in-line (IL) vibrations are the lack of test data with combined IL and CF response, and that CF response is regarded to cause more effect on fatigue failure than IL. Baarholm et al. [7] indicates, however, that fatigue damage due to IL vibrations may become significant for long cylinder structures.

The purpose of present work is to develop a model, following Wang et al. [8], Furnes and Sorensen [9], Violette et al. [10] and Ge et al. [11], to calculate IL and CF responses of the long tensioned cylinder under linearly shear flow conditions. In Sect. 2 of this paper, the model based on van der Pol oscillators in linearly shear flow is summarized. The coupling between IL and CF vibration and the structural geometric nonlinearity are accounted for. In Sect. 3, the results from wake oscillator model are verified with experimentally observed riser behavior [12]. The 4th section contains the comparison of results for uniform flow case and non-uniform flow case.

2 Model formulation

A Cartesian right-hand coordinate system is defined with x and y in the horizontal plane and z vertically upwards. Consider a free-span circular cylinder with uniform material properties and constant diameter D, which follows the z-axis and is pinned at two ends (Fig. 1).

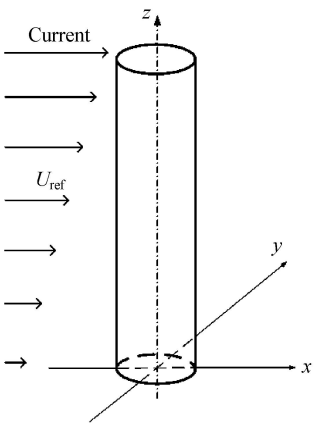

Fig. 1 Sketch of the cylinder with coordinate system

The related dynamic equations are

$$\begin{aligned} \bar{m}\frac{\partial^2 x}{\partial t^2} + (C + C')\frac{\partial x}{\partial t} + EI\frac{\partial^4 x}{\partial z^4} - \frac{\partial}{\partial z}\left(T\frac{\partial x}{\partial z}\right) &= F_x, \\ \bar{m}\frac{\partial^2 y}{\partial t^2} + (C + C')\frac{\partial y}{\partial t} + EI\frac{\partial^4 y}{\partial z^4} - \frac{\partial}{\partial z}\left(T\frac{\partial y}{\partial z}\right) &= F_y, \end{aligned} \tag{1}$$

where $\bar{m}$ is the sum of structure mass m_{s} and added fluid mass m_{f}, per unit length. Lacking a formulation of m_{f} varying with cylinder deflection, it is assumed that m_{f} is independent of time, $\bar{m}$ is hence given by

$$\bar{m} = m_{\text{s}} + \frac{\pi}{4}C_{\text{a}}\rho D^2, \tag{2}$$

where C_{a} is the added mass coefficient, ρ is the density of fluid and D is the diameter of cylinder. In Eq. (1), C and C' are the damping coefficients associated with structure and hydrodynamic forces, respectively. C' is related with vortex shedding frequency Ω_{f} and given by

$$C' = \gamma\Omega_{\text{f}}\rho D^2, \tag{3}$$

where γ is a parameter determined by experiment. In Eq. (1), EI is the bending stiffness of cylinder, T is the axial tension in cylinder which can be expressed by

$$T = T_0 + EA\frac{S - L}{L}, \tag{4}$$

where L and S are the initial length and instantaneous length of cylinder, respectively, T_0 is the initial value when $S = L$, E is Young's modulus of elasticity, A is the wall cross section area (stress area), and the elongation $S - L$ of the cylinder due to the deflections is computed from

$$\frac{\mathrm{d}S}{\mathrm{d}z} = \sqrt{1 + \left(\frac{\partial x}{\partial z}\right)^2 + \left(\frac{\partial y}{\partial z}\right)^2}. \tag{5}$$

Axial tension T is assumed to be independent of z, which is based on that the variation of T along the cylinder axis is much smaller than the variation due to the cylinder deflection [9].

In Eq. (1), F_x and F_y are the external hydrodynamic excitation forces due to the wake dynamics, which are expressed as

$$F_x = \frac{1}{2}C_{\text{D}}\rho DU^2, \qquad F_y = \frac{1}{2}C_{\text{L}}\rho DU^2, \tag{6}$$

where U is the current velocity acting normal to the cylinder and C_{D} and C_{L} are non-dimensional coefficients, which represent in-line drag and cross flow lift respectively. For a stationary cylinder these coefficients are fairly well documented as functions of Reynolds number, but as the cylinder starts to oscillate the structure deflection will affect the fluid and therefore the lift and drag coefficients. It has been found in experiment [13] that the drag coefficient increases with increasing cross flow amplitude, and the drag coefficient is

$$C_{\text{D}} = \bar{C}_{\text{D}} + \tilde{C}_{\text{D}} = C_{\text{D0}}\left(1 + K\frac{a_y}{D}\right) + C_{\text{D}i}, \tag{7}$$

where $\overline{C}_{\mathrm{D}}$ is the average drag coefficient, $\tilde{C}_{\mathrm{D}}$ is the pulsatory drag coefficient, C_{D0} is the drag coefficient for a cylinder at rest, K is a constant of magnitude 2, a_y is the amplitude of cross flow vibration and $C_{\mathrm{D}i}$ is a drag term as a function of time. $C_{\mathrm{D}i}$ and C_{L} are modeled by wake oscillator satisfying the van der Pol equation as done by Furnes and Sorensen [9], for which, a set of non-dimensional variables q_x and q_y are introduced

$$\begin{aligned}\frac{\partial^2 q_x}{\partial t^2}+\varepsilon_x\Omega_{\mathrm{f}}(q_x^2-1)\frac{\partial q_x}{\partial t}+4\Omega_{\mathrm{f}}^2 q_x&=\frac{A_x}{D}\frac{\partial^2 x}{\partial t^2},\\ \frac{\partial^2 q_y}{\partial t^2}+\varepsilon_y\Omega_{\mathrm{f}}(q_y^2-1)\frac{\partial q_y}{\partial t}+\Omega_{\mathrm{f}}^2 q_y&=\frac{A_y}{D}\frac{\partial^2 y}{\partial t^2},\end{aligned}\tag{8}$$

where q_x is in-line variable, q_y is cross flow variable, and the vortex induced drag and lift coefficients are correspondingly modeled by

$$C_{\mathrm{D}i}=C_{\mathrm{D}i0}\frac{q_x}{2},\qquad C_{\mathrm{L}}=C_{\mathrm{L}0}\frac{q_y}{2},\tag{9}$$

where $C_{\mathrm{D}i0}, C_{\mathrm{L}0}$ are vortex shedding drag and lift coefficients for a fixed rigid cylinder subjected to vortex shedding. In Eq. (8), $\varepsilon_x, \varepsilon_y, A_x$ and A_y are non-dimensional parameters estimated by experiment and Ω_{f} is the Strouhal frequency

$$\Omega_{\mathrm{f}}=2\pi S_t\frac{U}{D},\tag{10}$$

where S_t is the Strouhal number which is dependent on the Reynolds number.

By considering the spatial variation of the current, the cylinder is divided into N intervals which are bounded by coordinates $z_0, z_1, \cdots, z_N$ where z_0 is at the location of $z=0$ and z_N is at $z=L$. The current velocity varied linearly in each interval and for the interval $z_k < z < z_{k+1}$ the mean current velocity is then given by

$$\bar{V}_k=\frac{1}{\Delta L_k}\int_{z_k}^{z_{k+1}}(bz+c)\mathrm{d}z=\frac{b}{2}(z_{k+1}+z_k)+c_k,\tag{11}$$

where we assume that the current profile is linear shear. Since the current is allowed to vary in the axial direction, the vortex-shedding frequency will also vary in N line segments. This frequency is computed by Eq. (10). Although the current velocity varies linearly in each segment, the current velocity in Eq. (10) adopts the mean velocity of each segment.

The right-hand sides of Eq. (8) express the effects of cylinder motion on near wake. An acceleration coupling term is chosen as recommended by Faccinetti et al. [6].

For a cylinder at rest, the drag and lift forces coincide with the x- and y-axis, respectively, as shown in Fig. 2a. f_{D} is the average drag force acting on the cylinder with the average drag coefficient $\overline{C}_{\mathrm{D}}$. f'_{D}, f_{L} are the vortex induced drag and lift force, respectively, and contains the pulsatory drag coefficient $\tilde{C}_{\mathrm{D}}$ (or $C_{\mathrm{D}i}$) and the lift coefficient C_{L} individually in its expression as Eq. (6). When the cylinder starts to vibrate as a result of vortex shedding, the drag and lift forces do not coincide with the x- and y-axis any more, which is shown in Fig. 2b. The corresponding forces exerted on the cylinder can thus be expressed as

$$\begin{aligned}F_x&=f_{\mathrm{D}}+f'_{\mathrm{D}}\cos\theta-f_{\mathrm{L}}\sin\theta,\\ F_y&=f_{\mathrm{L}}\cos\theta+f'_{\mathrm{D}}\sin\theta,\end{aligned}\tag{12}$$

where θ is the angle between x-axis and the instantaneous velocity of the cylinder, such that

$$\theta(t)=\arctan\Big(\frac{\dot{y}(t)}{U-\dot{x}(t)}\Big)=\arctan\Big(\frac{\dot{Y}(t)}{1-\dot{X}(t)}\Big),\tag{13}$$

where the dot denotes differentiation with respect to time, $\dot{X}, \dot{Y}$ are non-dimensional velocities. Since, in general, $\dot{X}, \dot{Y}$ are smaller than 1, the angle θ is very small and

$$\begin{aligned}\sin\theta(t)&=\frac{\dot{Y}(t)}{\sqrt{\dot{Y}^2(t)+(1-\dot{X}(t))^2}}\approx\dot{Y}(t),\\ \cos\theta(t)&=\frac{1-\dot{X}(t)}{\sqrt{\dot{Y}^2(t)+(1-\dot{X}(t))^2}}\approx 1.\end{aligned}\tag{14}$$

Substituting Eq. (14) into Eq. (12), we get the formulation of the right-hand sides in Eq. (1)

$$\begin{aligned}F_x&=f_{\mathrm{D}}+f'_{\mathrm{D}}-f_{\mathrm{L}}\dot{Y}(t),\\ F_y&=f_{\mathrm{L}}+f'_{\mathrm{D}}\dot{Y}(t).\end{aligned}\tag{15}$$

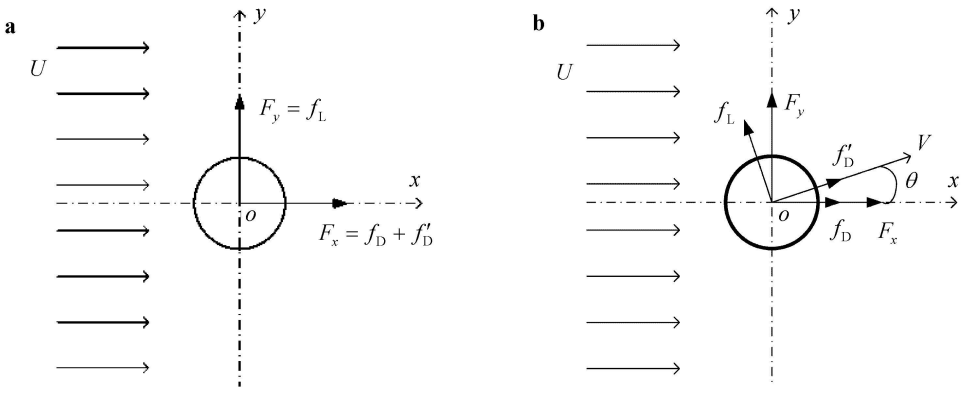

Fig. 2 Illustration of one cross-section of a cylinder in a cross flow and the fluid forces exerted on it. **a** Stationary cylinder; **b** Vibrating cylinder

3 Comparison with experimental results

In this section, the focus is on evaluating the capability of the wake oscillator model to predict some experimentally observed results on long flexible structures. Baarholm et al. [7] and Lie and Kaasen [12] presented a summary of a large experimental campaign, where a tensioned large-scale riser model was tested at Hanøytangen outside Bergen on the west coast of Norway in 1997. Figure 3 shows a simplified illustration of their experimental setup.

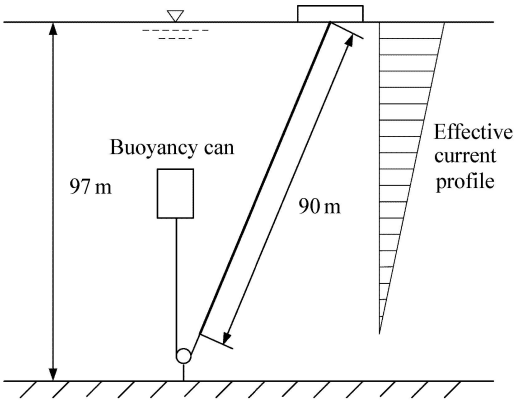

Fig. 3 Test set-up at Hanøytangen [12]

As seen in Fig. 3, by moving the vehicle at a constant velocity, the riser was exposed to a triangular current profile. In this way, a well-defined current profile was obtained. The characteristics of the riser are listed in Table 1. The riser model has a mass ratio (mass/mass of displaced water) of 3.13 and a length diameter ratio of 3 000.

Table 1 Riser characteristics

Structural properties	Value
Length	$L = 90\,\text{m}$
Outer diameter	$D = 0.03\,\text{m}$
Inner diameter	$t = 0.026\,\text{m}$
Structure mass	$m_s = 2.27\,\text{kg/m}$
Young's modulus	$E = 2.1 \times 10^{11}\,\text{N/m}^2$
Axial tension	$T = 3.7\,\text{kN}$

Although the Strouhal number is dependent on Reynolds number, it is here taken as constant, which is assumed to be a fairly reasonable approximation for the subcritical range. For a cylinder undergoing vibration, the Strouhal number is set as 0.17. This value is lower than the usually quoted 0.2, but has been found to apply for moving cylinders [12]. The added mass coefficient C_a is dependent on current velocity, vibration amplitude and frequency. Since there is no efficient way for estimating the variations, for a cylinder, the value of C_a is taken of 1.0.

The values of C_{D0}, C_{Di0} and C_{L0} all depend on Reynolds number, which are given as $C_{D0} = 1.2, C_{Di0} = 0.1$ and $C_{L0} = 0.3$, respectively, for a rigid cylinder at the subcritical range [9]. Values for the coefficients in Eq. (8) were recommended by Facchinetti et al. [6] as $\varepsilon_x = 0.3$, $\varepsilon_y = 0.3$, $A_x = 12$ and $A_y = 12$. Due to the relation of these parameters to intrinsic wake dynamics, the recommended values must be verified since they are deduced from experimental data on forced oscillation vortex shedding only. Through tuning of the model the same ε value was obtained, while $A_x = 12$ and $A_y = 36$ was chosen for the best fit with the experimental results.

This system is numerically integrated with respect to time and space using a standard centered finite differential method of the second order in both domains. The riser is divided into segments with the length of 0.5 m, which is sufficient to describe the largest excited mode of riser vibration. The time step used in the calculation is chosen much smaller than the minimum vibration period of riser considered in this case and the calculation convergence was checked. The initial conditions of the system are expressed by

$$x(z,0) = y(z,0) = 0, \qquad \frac{\partial x(z,0)}{\partial t} = \frac{\partial y(z,0)}{\partial t} = 0, \tag{16}$$

$$q_x = q_y = 2, \qquad \frac{\partial q_x}{\partial t} = \frac{\partial q_y}{\partial t} = 0. \tag{17}$$

Equation (16) means zero displacement and velocity of initial conditions are applied to the riser. As for wake oscillator, it is assumed that the initial values of fluid variables are equal to 2.0, and the first derivatives with respect to time are set to zero. Pin end conditions are employed at either end of the riser, which means the displacements and bending moments are equal to zero at $z = 0$ and $z = L$.

To verify the results computed with the wake oscillator model, we make comparisons with experimental data [12], where the constant speed at upper riser end varies between 0.16–2 m/s. The same conditions are used in numerical simulation. As an example, Fig. 4 shows the root mean square (RMS) values of the CF displacement along the riser when the towing speed is equal to 0.54 m/s. Solid line represents the wake oscillator simulation, and it generally fits the experimental data of dotted curve. Both simulation and test result indicate the presence of the 11th mode, and the riser response is a combination of traveling and standing waves, which is also shown in Fig. 5 that presents the time evolution of riser CF displacement at every span computed by the wake oscillator model. We observe that the traveling wave appears away from the riser ends and the standing wave is dominant near the ends due to the boundary conditions.

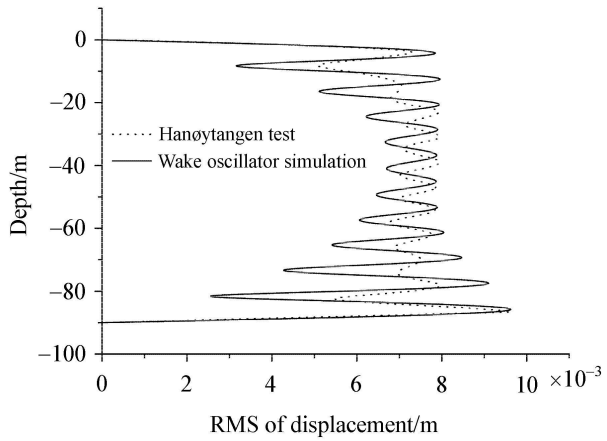

Fig. 4 Comparison of CF RMS of displacement when towing speed is 0.54 m/s

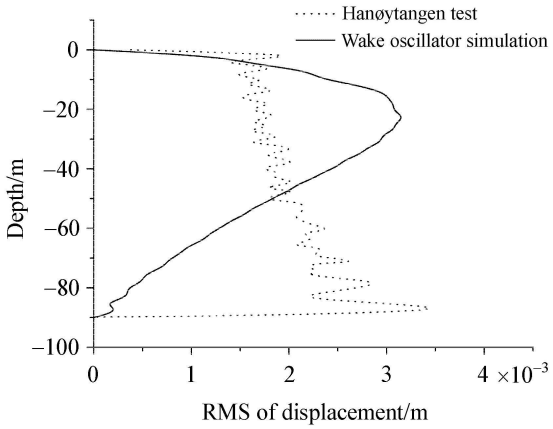

Fig. 6 Comparison of IL RMS of displacement when towing speed is 0.54 m/s

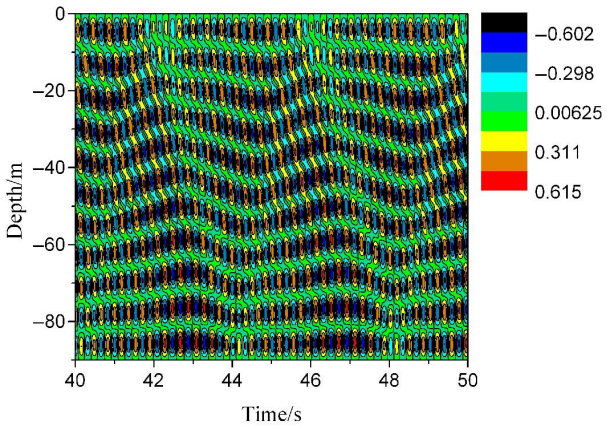

Fig. 5 Evolution of riser CF displacement with time and space when towing speed is 0.54 m/s

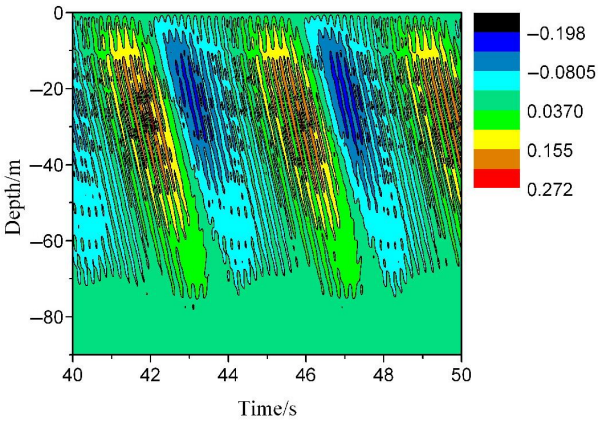

Fig. 7 Evolution of riser IL displacement with time and space when towing speed is 0.54 m/s

Figure 6 shows the results of IL VIV, which deviates from the experimental data. The test result shows that riser response is also a combination of traveling and standing waves. For small size ripples, the response mainly consists of traveling waves. The dominant mode is number 23 and its frequency is 5.4 Hz [12]. Nevertheless the wake oscillator simulation shows that traveling wave is dominating. In Fig. 7 one can observe that the excitation takes place in the upper region, where the current velocity has the maximum value and the energy is transferred from fluid to the riser. Then the downward traveling wave is damped quickly before it arrives at the bottom end. It is clear that once the wave has propagated away from the location where it is generated, the energy is transferred back to the fluid which actually offers the damping effect. The traveling wave has a frequency of approximately twice of local Strouhal frequency based on the upper region current velocity and the frequency remains constant when the wave travels along the riser.

Figures 8–10 show some key parameters as functions of the towing speed, which varied from 0.16–1.14 m/s. One measure of the magnitude of the VIV is the average RMS taken over the length of the riser. Figure 8 presents this for CF and IL responses. Solid square and circular symbols represent experimental data, hollow square and circular symbols represent computed data by wake oscillator model. The comparison shows that the wake oscillator simulation fits with the test data for both CF and IL VIVs. The average RMS values of IL and CF displacements vary only a little with the towing speed.

Figure 9 shows how the vibration frequency of CF and IL VIVs varies with the towing speed. Vibration frequency here means the dominant frequency taken from the spectrum of displacement at the riser midspan. The symbol definitions are the same with Fig. 8. It is clear that both test and simulation results show an increasing trend with the towing speed. The lower straight line is the Strouhal frequency, based on the towing speed and a Strouhal number of 0.17. The upper segment line represents twice the Strouhal frequency. The

two straight lines approximately fit both the test and simulation data. This means that the IL vibration frequency is almost twice the CF vibration frequency.

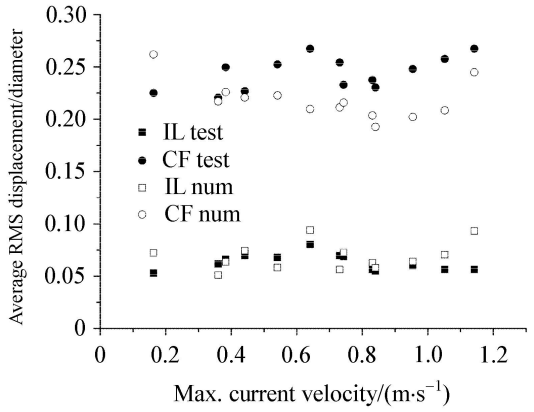

Fig. 8 Comparison of average RMS values of displacement at different towing speeds

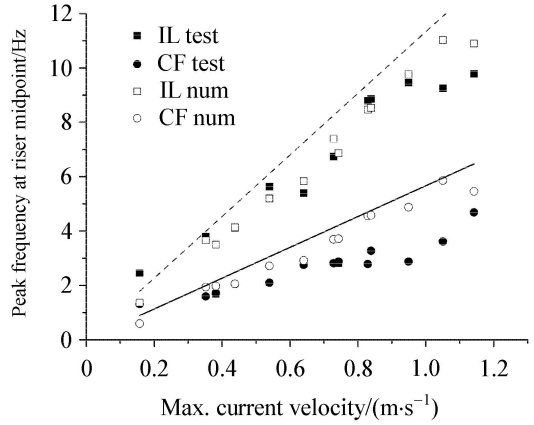

Fig. 9 Comparison of vibration frequencies at different towing speeds

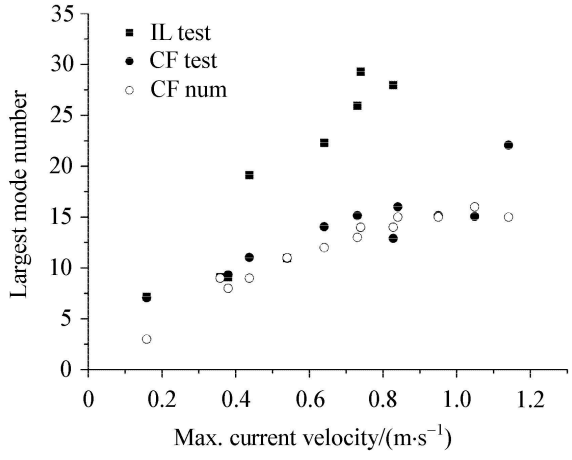

Fig. 10 Comparison of dominant mode numbers at different towing speeds

Figure 10 presents the comparison of the number of dominating mode with respect to displacement in both CF and IL vibrations. The numerical results for IL response are not included here, because traveling waves are dominating in IL vibration, hence the mode shape of the standing wave is hard to be identified. Nevertheless it appears from the figure that the number of dominating mode for CF vibration fits the experimental data and increases linearly with the towing speed.

In this case, the average values of IL amplitude are only about one quarter of values of CF. It means that the frequency of vibration in the IL possibly does not align with any natural frequency of riser therefore the riser responds with small amplitude. As we know, the riser with axial tension has two main regimes of natural frequencies. One regime is dominated by the axial tension where it is like a tensioned string and the other is dominated by the bending stiffness where it is similar to a beam. Figure 11 presents the natural frequencies of a string, beam and riser which have the same mass and boundary conditions. For modes up to the 8th, the natural frequency of the tensioned string and the riser are virtually identical and it is proportional to the mode number. From the 11th mode and higher, the natural frequency is seen to follow the same trend as the beam then it is proportional to the mode number squared. As referred to Swithenbank and Larsen [14], if the mode number of CF is higher than 4th, there may be an available natural frequency at twice the CF frequency, but that is not guaranteed. Therefore if the frequency of IL is not on or near a natural frequency of the riser, the amplitude of the IL vibration will significantly decrease. It is seen from Fig. 10 that the mode number of CF during the tests is always higher than 5th. Considering the small energy transferred from the wake and the fluid damping effect, we are convinced that when the frequency of IL vibration does not align with a natural frequency, the standing wave is hard to be persistent. It may be the reason that the characteristics of standing wave in IL are not available to be identified in this simulation with wake oscillator.

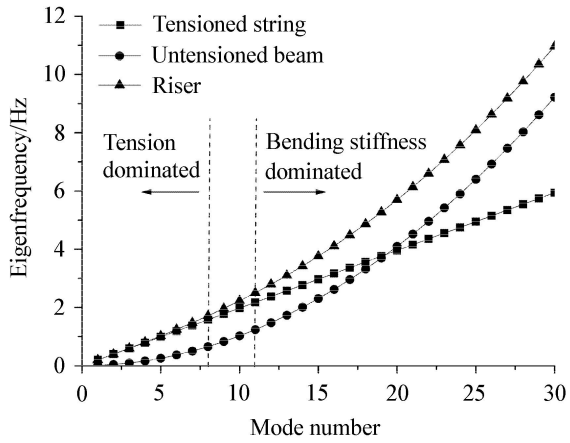

Fig. 11 Natural frequencies of three different systems

On the other hand, the added mass is assumed to be constant in the simulation. However the added mass is frequency dependent. This allows for the different added masses for the IL and CF vibrations, respectively, which will influence the natural frequency and has a potential to align it with the frequency of vibration. Therefore in the model test, the standing wave is possible to be identified in some cases as shown in Fig. 10.

4 Vibrations in uniform flow

In non-uniform flows, the excitation bandwidth and the extent of lock-in are strongly influenced by the type and the magnitude of shear characteristics [15]. If the incident flow is steady in time and linearly sheared as shown in Fig. 1, the flow velocity is

$$U(z) = U_{\text{ref}}\left[1 + \beta\left(\frac{z}{L} - \frac{1}{2}\right)\right], \tag{18}$$

where U_{ref} is the velocity at the mid-span of structure and β is the incident flow shear parameter which is non-dimensional. To understand the effect of flow shear characteristics on the riser VIV, we consider an extremity case, where the incident flow is uniform along the span and hence the shear parameter reaches its minimum value. Here we set the velocity of uniform flow as the value of U_{ref}. Therefore when the towing speed is 0.54 m/s in the preceding case, the corresponding uniform flow velocity is 0.27 m/s. The simulation of riser VIV is also performed with the same wake oscillator model and the results are made comparison with the associated shear flow case.

Figures 12 and 13 show the RMS values of the CF and IL displacements along the riser, respectively. The RMS values in linearly shear flow are also presented in both figures. It is clear that the riser response in uniform flow is a combination of traveling wave and standing wave in IL or CF direction. Comparing with the CF response in linearly shear flow, one notices that the excited riser modes are different. In uniform flow the excited mode number is 7th, while in shear flow the dominant mode number is 11th. Moreover the amplitude in uniform flow is larger than it in shear flow, which may be interpreted by considering the varied size of lock-in region as the different flow shear parameters. As the flow shear parameter increases the extent of local lock-in along the span of riser reduces [16], which means the energy transferred from the wake into the riser reduces, so that the amplitude of riser vibration decreases.

In Fig. 13, the riser response in linearly shear flow shows that the traveling wave is dominant. The wave is excited at the upper part of the riser and gets damped as it propagates downwards. It means that energy is inputted to the riser in a certain location where the fluid coefficient in phase with velocity is positive, and then the energy is transferred to adjacent areas where the velocity of the current is different and the same coefficient is negative. Hence the propagating energy is dissipated at these adjacent areas. Shear flow exhibits this phenomenon, while uniform flow does not.

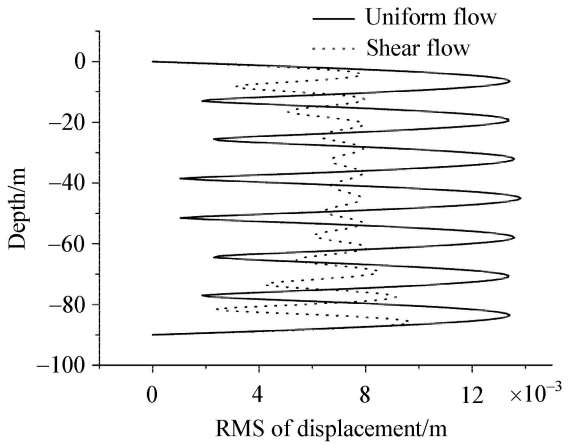

Fig. 12 Comparison of CF displacement RMS under uniform and shear flow conditions

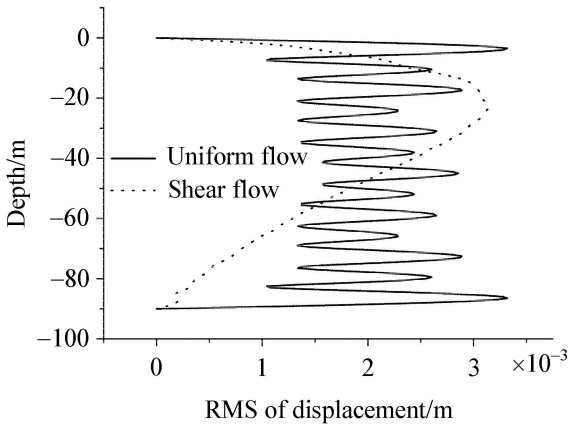

Fig. 13 Comparison of IL displacement RMS under uniform and shear flow conditions

Figure 14 shows the effect of the flow shear characteristics on the number of modes contributing to the response of the riser. A single dominant peak is presented in Fig. 14a. This means that for uniform flow case the riser response is dominated by a single frequency and characterized by a single vibration mode. Nevertheless there are multiple frequency peaks in linearly shear flow case as show in Fig. 14b. Multiple peaks suggest that the riser response in shear flow is a multi-mode response. It was also reproduced by Violette et al. [10] and Lucor and Triantafyllou [15] that the transition from multimode to single-mode response is due to the variation of flow shear parameter.

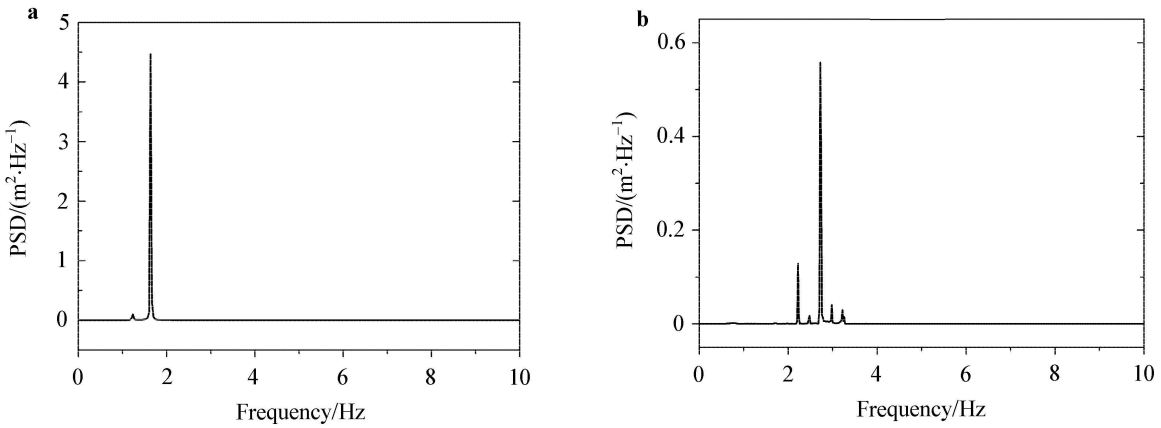

Fig. 14 PSD of CF displacement at midspan of riser. **a** Uniform flow case and $U = 0.27$ m/s; **b** Linearly shear flow case and $U_{\text{tow}} = 0.54$ m/s

5 Conclusions

A three dimensional model is presented to formulate the vortex-induced vibrations of a long circular cylinder placed in shear flow, similar to the type of riser or tension leg. Wake oscillator model based on van del Pol equation is used to simulate the wake dynamics in the CF direction and extended to the IL direction. The oscillators are distributed along the cylinder. The vortex shedding frequency is derived from local current velocity. Correlation effect between adjacent oscillators along the span is ignored. Coupling effect due to cylinder vibration on the wake oscillator is modeled by the acceleration of cylinder. Moreover the coupling term between IL and CF fluid forces is introduced to reflect the relative motion of cylinder to current.

Validations of the simulation against experimental data show that the presented model can simulate some dynamic features of long slender cylinder VIV in shear flow. The spanwise average RMS displacement does not increase with towing speed. The vibration frequency of CF or IL approximately fit the Strouhal frequency and increases with towing speed. A principle feature of riser modes of CF is that they are combination of standing and traveling waves while in IL direction the traveling wave is dominant in most cases. The difference of vibration mode of IL between simulation and experiment is related with whether the influence of varied added mass is considered or not. Comparing with uniform flow case, we draw a conclusion that the incident flow profile has significantly influenced the vibration characteristics of riser including the vibration amplitude, extent of frequency range, excited mode number and so on. The presented model also reproduces the transition from multimode to single-mode response due to the variation of current velocity profile.

In addition, because of the simplicity of the model, all the results presented in this paper require only a few hours of CPU time on a PC. This means that the present model is efficient to undertake comprehensive parametrical studies for VIV of long cylinders.

References

1 Marcollo, H., Hinwood, J.B.: On shear flow single mode lock-in with both cross-flow and in-line lock-in mechanisms. Journal of Fluids and Structures **22**(2), 197–211 (2006)
2 Sarpkaya, T.: A critical review of the intrinsic nature of vortex-induced vibrations. Journal of Fluids and Structures **19**(4), 389–447 (2004)
3 Williamson, C.H.K., Govardhan, R.: Vortex-induced vibrations. Annual Review of Fluid Mechanics **36**, 413–455 (2004)
4 Gabbai, R.D., Benaroya, H.: An overview of modeling and experiments of vortex-induced vibration of circular cylinders. Journal of Sound and Vibration **282**(3-5), 575–616 (2005)
5 Chaplin, J.R., Bearman, P.W., Cheng, Y., et al.: Blind predictions of laboratory measurements of vortex-induced vibrations of a tension riser. Journal of Fluids and Structures **21**(1), 25–40 (2005)
6 Facchinetti, M.L., de Langre, E., Biolley, F.: Coupling of structure and wake oscillator in vortex-induced vibrations. Journal of Fluids and Structures **19**(2), 123–140 (2004)
7 Baarholm, G.S., Larsen, C.M., Lie, H.: On fatigue damage accumulation from in-line and cross-flow vortex-induced vibrations on risers. Journal of Fluids and Structures **22**(1), 109–127 (2006)
8 Wang, X.Q., So, R.M.C., Chan, K.T.: A non-linear fluid force model for vortex-induced vibration of an elastic cylinder. Journal of Sound and Vibration **260**(2), 287–305 (2003)
9 Furnes, G.K., Sorensen, K.: Flow induced vibrations modeled by coupled non-linear oscillators. In: Chung, J.S., Hong, S.W., Nagata, S. et al eds. Proceedings of the 17th International Offshore and Polar Engineering Conference, Lisbon, Portugal, July 1-6, 2007. Cupertino: ISOPE, **3**, 2781–2787 (2007)
10 Violette, R., de Langer, E., Szydlowski, J.: Computation of vortex-induced vibrations of long structures using a wake oscillator model: Comparison with DNS and experiments. Computers & Structures **85**(14), 1134–1141 (2007)

11 Ge, F., Long, X., Wang, L., et al.: Flow induced vibrations of long circular cylinders modeled by coupled non-linear oscillators. Science in China Series G: Physics, Mechanics & Astronomy **52**(7), 1086–1093 (2009)
12 Lie, H., Kaasen, K.E.: Modal analysis of measurements from a large-scale VIV model test of a riser in linearly sheared flow. Journal of Fluids and Structures **22**(4), 557–575 (2006)
13 Sarpkaya, T.: Fluid forces on oscillating cylinders. Journal of the Waterway Port Coastal and Ocean Division **104**(3), 275–290 (1978)
14 Swithenbank, S.B., Larsen, C.M.: The importance of mode number on in-line amplitude of vortex-induced vibration of flexible cylinders. In: Soares C.G. ed. Proceedings of the ASME 27th International Conference on Offshore Mechanics and Arctic Engineering, Estoril, Portugal, June 15-20, 2008. New York: ASME, **5**, 771–778 (2008)
15 Lucor, D., Triantafyllou, M.S.: Riser response analysis by modal phase reconstruction. Journal of Offshore Mechanics and Arctic Engineering **130**(1), 011008/1–011008/9 (2008)
16 Mathelin, L., de Langre, E.: Vortex-induced vibrations and waves under shear flow with a wake oscillator model. European Journal of Mechanics B/Fluids **24**(4), 478–490 (2005)